Retrieving plasmonic near-field information: A quantum-mechanical model for streaking photoelectron spectroscopy of gold nanospheres

Jianxiong Li, Erfan Saydanzad, and Uwe Thumm

Phys. Rev. A **94**, 051401 — Published 14 November 2016

DOI: 10.1103/PhysRevA.94.051401

Retrieving plasmonic near-field information: a quantum-mechanical model for streaking photoelectron spectroscopy of gold nanospheres

Jianxiong Li, Erfan Saydanzad, and Uwe Thumm
Department of Physics, Kansas State University, Manhattan, Kansas 66506, USA

Streaked photoemission from nanostructures is characterized by size and material dependent nm-scale variations of the induced nanoplasmonic response to the electronic field of the streaking pulse and thus holds promise to allow photoelectron imaging with both, sub-fs temporal and nm spatial resolution. In order to scrutinize the driven collective electronic dynamics in 10 to 200 nm diameter gold nanospheres, we calculated the plasmonic field induced by streaking pulses in the infrared (IR) and visible spectral range and developed a quantum-mechanical model for streaked photoemission by extreme ultraviolet (XUV) pulses. Our simulated photoelectron spectra reveal a significant amplitude enhancement and phase shift of the photoelectron streaking trace relative to calculations that exclude the induced plasmonic field. Both are most pronounced for streaking pulses tuned to the plasmon frequency and retrace the plasmonic electromagnetic field enhancement and phase shift near the nanosphere surface.

PACS numbers: 73.20.Mf, 78.20.Bh, 78.47.J-

Recent advances in nano-science and nano-technologies are creating new avenues for designing and making nanometer-scale metal structures which respond to irradiation with electromagnetic radiation by creating a tunable induced electric field near the metal surface [1, 2]. This induced "plasmonic" field originates in the incident-field driven coherent collective motion of conduction electrons which, when stimulated near its natural resonance (plasmon) frequency, generate a very large induced polarization in sub-wavelength-size structures on substrate surfaces [3–9] and isolated nanopaticles [10]. Near metallic nanospheres and for linearly polarized incident radiation [10–16], the oscillating induced polarization gives rise to oscillating plasmonic fields with dipole-like angular distribution oriented along the polarization direction of the incident radiation [17].

Strong plasmonic field enhancement effects are linked to the local dielectric properties of the nanostructure and form the underlying physical phenomenon in established surface-enhanced Raman spectroscopy (SERS) [18] and various prototype and suggested applications, such as attosecond nanoplasmonic-field microscopy [3] and nanoplasmonically enhanced photocatalysis [19] and light harvesting [20]. The detailed understanding of plasmonic excitations in solids requires imaging techniques that resolve their spatio-temporal evolution [3, 16]. While ultrafast laser technology is available in many laboratories wordwide, allowing the resolution of various aspects of the electronic dynamics during the IR-pulse-streaked XUV photoionization of gaseous atoms with a precision of about 10 attoseconds [21], a promising emerging line of attosecond science targets the electronic dynamics in solids, bio-molecules, and nanostructures [2, 22]. These highly time-resolved investigations on solid targets address effects that are absent in isolated atoms in the gas phase, such as the propagation of photo-excited electrons in the solid, accompanied by elastic and inelastic scattering [23, 24], the emitted photoelectron's interaction with equilibrating residual surface-charge distributions [25], and the inhomogeneous nanoplasmonic enhancement [10, 12–16] and finite skin depth [26] of the incident IR pulse in photoelectron streaking measurements.

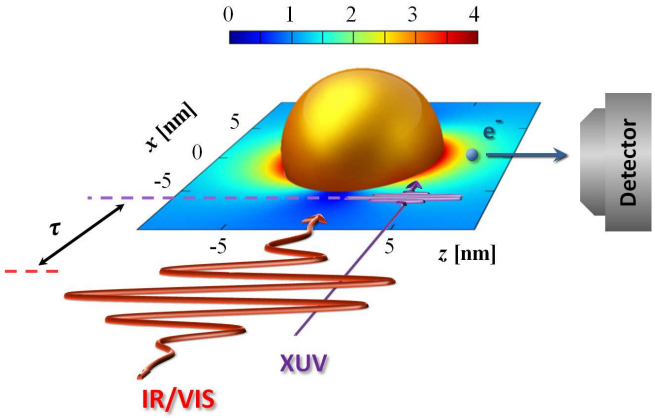

Figure 1. (Color online) Schematic of attosecond streaking from nanoparticles. A single attosecond XUV pulse emits electrons into the field of a delayed IR streaking laser pulse. The linear color scale represents the local electric-field-strength enhancement $\eta(\mathbf{r})$ in the $x-z$ plane for a 100 nm diameter Au nanosphere.

We have developed a single-active-electron quantum-mechanical model for calculating streaked XUV-photoemission spectra from Au nanospheres with diameters below the wavelength of the streaking light (Fig. 1). Our simulated spectra show strong amplitude enhancements and phase shifts of the photoelectron streaking trace that match the field enhancement and phase shift of the plasmonically enhanced streaking field. Our quantum-mechanical numerical model thus confirms the possibility of imaging the plasmonic field distribution near nanostructures in streaked electron spectra predicted by previous classical-mechanics simu-

lations [10, 12–15]. Throughout this work we use atomic units (a.u.) unless stated otherwise and assume the XUV and streaking pulses are incident along the x-axis and linearly polarized along the z-axis of our coordinate system with origin at the center of the nanosphere.

We consider electron emission from the conduction band of a metal nanosphere of diameter D by isolated XUV pulses into the field of a delayed IR or visible light pulse (Fig. 1). For streaked photoemission to occur, the XUV pulselength τ_X is assumed to be short compared to the period of the streaking pulse. The streaking pulse intensity assumed in our numerical applications below is too small to ionize the nanoparticle, yet causes a measurable energy shift of the photoelectron's final energy $\varepsilon_f(\tau)$ as a function of the delay τ of the streaking relative to the XUV pulse [16]. This shift is due to the acceleration of the photoelectron in the total electric field $\mathbf{E}_{tot}$ which is composed of the spatially homogenous incident streaking field $\mathbf{E}_{inc}$ and the inhomogenious plasmonic field $\mathbf{E}_{plas}$ it induces in the nanosphere. $\varepsilon_f(\tau)$ further depends on characteristics of the XUV pulse and the size- and frequency-dependent local dielectric response of the nanosphere [17, 27]. Detection of $\varepsilon_f(\tau)$ thus reveals information on the plasmonic field and dielectric properties of the sphere.

For incident plane waves $\mathbf{E}_{inc}(\mathbf{r},t;\omega) = \hat{\mathbf{z}}E_0(\omega)\ e^{i(kx-\omega t)}$, we solved Maxwell's equations for the inhomogeneous total electric field

$$\begin{aligned}\mathbf{E}_{tot}(\mathbf{r},t;\omega) &= \mathbf{E}_{inc}(\mathbf{r},t;\omega) + \mathbf{E}_{plas}(\mathbf{r},t;\omega)\\ &= \mathbf{E}_{tot,0}(\mathbf{r};\omega)\ e^{i\phi_{tot}(\mathbf{r};\omega)}\ e^{-i\omega t} \qquad (1)\end{aligned}$$

in terms of an infinite series expansion and determined the expansion coefficients from the boundary conditions at the sphere's surface, following Mie [17, 28]. The largest electric-field enhancement $\eta(\mathbf{r}) = |\mathbf{E}_{tot,0}(\mathbf{r};\omega)|/E_0$ occurs at the electric-field "poles" [$\mathbf{r}_p = (0,0,z_p)$] of the sphere along the polarization direction and is shown in Fig. 2(a) for 10 to 200 nm diameter Au spheres and 400 to 900 nm wavelength incident plane waves, based on experimentally determined complex refraction indices $n(\omega)$ for bulk Au [27]. $\eta(\mathbf{r}_p)$ and the local phase shift relative to the incident wave, $\Delta\phi(\mathbf{r}_p) = \phi_{tot}(\mathbf{r}_p;\omega) - kz_p$ [Fig. 2(b)], are strongly enhanced at the Au plasmon resonance which strongly red shifts for $D > 100$ nm from 500 to 530 nm [27] in agreement with previous calculations [12] and measured photo-absorption spectra [29]. For $\lambda >> D$, $\Delta\phi_{tot}(\mathbf{r}_p)$ vanishes as conduction electrons adiabatically follow the driving external field.

By superimposing spectral components $\mathbf{E}_{tot}(\mathbf{r},t;\omega)$, we include in

$$\mathbf{E}_{tot}(\mathbf{r},t) = \int d\omega \mathbf{E}_{tot,0}(\mathbf{r};\omega)\ e^{i\phi_{tot}(\mathbf{r};\omega)}\ e^{-i\omega t} \qquad (2)$$

the induced plasmonic response of Au nanoparticles to streaking pulses with Gaussian temporal profiles, 2.47 fs full width at half intensity maximum (FWHIM), corresponding to a spectral width of $\Gamma_{inc} = 0.73$ eV, and 10^{12} W/cm^2 peak intensity.

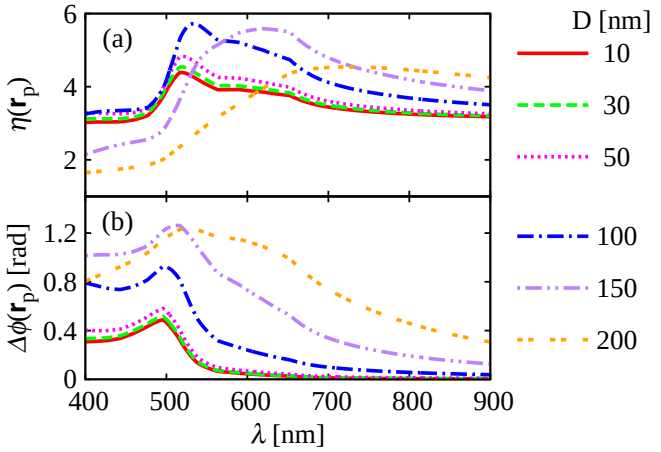

Figure 2. (Color online) (a) Plasmonic field enhancement $\eta(\mathbf{r}_p)$ and (b) phase shift $\Delta\phi(\mathbf{r}_p)$ at the electric-field poles $\mathbf{r}_p$ of Au nanospheres with diameters D as a function of the incident plane wave's wavelength λ.

We consider photoemission by the electric field

$$\mathbf{E}_X(t) = \hat{\mathbf{z}}E_X \exp\left[-2\ln 2\left(\frac{t-t_x}{\tau_X}\right)^2\right] e^{-i\omega_X(t-t_x)}, \quad (3)$$

of isolated XUV pulses with a Gaussian temporal profile, 105 eV photon energy, and $\tau_X = 200$ as pulse length (FWHIM), where $t_x = x/c$. Since $n(\omega) \approx 1$ at XUV frequencies, c can be taken as the vacuum speed of light, and the XUV-pulse vector potential (in Coulomb gauge) is given by $\mathbf{A}_X(t) = \int_t^\infty dt' \mathbf{E}_X(t')$.

XUV pulse intensities in typical streaking experiments result in single-XUV photon photoionization [16]. To first order in E_X, the photoemission amplitude for this process in the velocity gauge as a function of the final photoelectron momentum $\mathbf{k}_f$ and time delay τ is [26]

$$T_i(\mathbf{k}_f,\tau) \sim \int dt \int d\mathbf{r} \Psi^{\tau *}_{\mathbf{k}_f}(\mathbf{r},t)\mathbf{A}_X(\mathbf{r},t)\cdot\hat{\mathbf{p}}\Psi_i(\mathbf{r},t). \quad (4)$$

We model the initial conduction-band state $\Psi_i(\mathbf{r},t)$ in (4) as a stationary state in a spherical square well of radius $D/2$. The depth of the spherical square-well potential is assumed to equal the sum of the work function (5.1 eV [30]) and conduction-band width (8 eV [31]) of bulk Au. We represent the final state as the exponentially damped "Volkov" continuum wave function [26]

$$\Psi^{\tau}_{\mathbf{k}_f}(\mathbf{r},t) = \frac{1}{\sqrt{2\pi}} f[l(\mathbf{r});\lambda_i] e^{i\mathbf{k}_f\cdot\mathbf{r}} e^{i\phi^{\tau}_{\mathbf{k}_f}(\mathbf{r},t)} \qquad (5)$$

with the position-dependent generalized Volkov phase $\phi^{\tau}_{\mathbf{k}_f}(\mathbf{r},t) = \int_t^\infty dt' \mathbf{p}^2(\mathbf{r},t')/2$. The damping function $f(l;\lambda) = exp[-l/(2\lambda)]$ describes that photoelectrons which are excited ("born") by the XUV pulse at positions $\mathbf{r}$ inside the nanosphere and subsequently elastically or inelastically scattered before leaving the nanoparticle

surface are not registered by the TOF detector (Fig. 1). $f(l;\lambda) = exp[-l/(2\lambda)]$ depends on the energy-dependent inelastic mean free path (MFP) λ_i and the path length $l(\mathbf{r})$ of photoelectrons inside the nanosphere.

For 80 to 120 eV photoelectrons considered in this work, the MFP changes by about 2% [32] and is approximated by the constant value $\lambda_i \approx 4.4$ Å, such that only photoelectrons released within approximately 1 nm beneath the surface contribute to the streaked spectra. This relaxes our above assumption of XUV-transparent nanoparticles to a few atomic layers. $l(\mathbf{r})$ is calculated based on classical photoelectron trajectories $\tilde{\mathbf{r}}(t')$ with initial positions $\tilde{\mathbf{r}}(t) = \mathbf{r}$ at time t and initial momenta

$$\mathbf{p}(\mathbf{r},t) = \mathbf{k}_f + \int_t^\infty dt' \mathbf{E}_{tot}[\tilde{\mathbf{r}}(t'),t']. \tag{6}$$

Assuming that photoelectrons are detected in a very small solid angle around $\mathbf{k}_f$, the photoionization probability is obtained as a sum over occupied initial states with energies ε_i at and below the Fermi energy

$$P(\varepsilon_f,\tau) = \sum_{i\in occ} |T_i(\mathbf{k}_f,\tau)|^2. \tag{7}$$

For all numerical applications, we assume photoemission along the XUV polarization direction so that $\mathbf{k}_f = (0,0,k_f)$.

Figures 3(a)-3(d) show our simulated attosecond streaked photoelectron spectra for 10 and 50 nm diameter Au nanospheres and streaking pulses with central wavelengths of 720 and 530 nm. The simulated spectra retrace the temporal profile of the streaking electric field. For a given streaking-pulse wavelength λ, the streaking-oscillation amplitude $\delta\varepsilon_f(D,\lambda)$ increases with the size of the nanosphere, consistent with the size-dependent plasmonic streaking-field enhancement shown in Fig. 2(a). In contrast, for a given nanosphere diameter, $\delta\varepsilon_f$ at 720 nm in Figs. 3(a) and 3(c) is approximately equal to the respective amplitudes for 530 nm in Figs. 3(b) and 3(d), due to the cancelation of two effects. While for atomic targets the photoemission amplitude (4) with final states (5) implies $\delta\varepsilon_f(D,\lambda) \sim \lambda \times E_0$ [16], predicting a larger streaking amplitude at $\lambda = 720$ nm, the induced plasmonic field of the nanosphere results in $\delta\varepsilon_f(D,\lambda)$ being proportional to $\lambda \times |\mathbf{E}_{tot,0}|$. The smaller induced plasmonic-field contribution to $\mathbf{E}_{tot,0}$ at 720 nm in comparison with the plasmon-resonance-enhanced streaking-field amplitude at 530 nm thus offsets the decrease of $\delta\varepsilon_f$ with increasing λ that is well-known for gaseous atomic targets.

Figure 3(e) shows classical-trajectory simulations for 10 nm diameter Au nanospheres [12] for the same streaking and XUV-pulse parameters as Fig. 3(a). With regard to their overall shape, these classically calculated spectra are in fair agreement with our results. However, they show a noticeable difference in oscillation amplitude and phase. This may suggest that the coherent interaction of photoelectrons, which is not included in

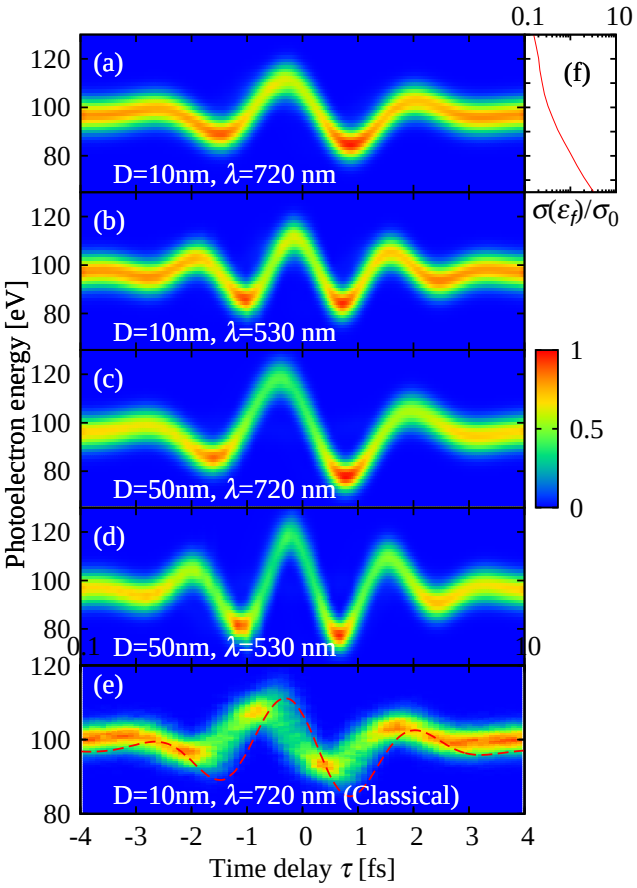

Figure 3. (Color online) Streaked XUV photoemission spectra for (a),(b) 10 nm and (c),(d) 50 nm diameter Au nanospheres and streaking-field wavelengths of (a),(c) 720 nm and (b),(d) 530 nm. The linear color/gray scale gives the photoemission yield normalized to the maximal yield in (a)-(d). (e) Classical simulation results by Süßmann and Kling [12]. The red dashed line shows the CoE of our corresponding quantum calculation in (a). (f) Photoionization cross section $\sigma(\varepsilon_f)$, normalized at $\sigma_0 = \sigma(80\ eV)$.

classical model, has a noticeable influence on streaked spectra. The spectra in Ref. [12] and our results also differ in an approximately 4 eV higher streaking-trace center of energy (CoE) in the classical model, due to the restriction in Ref. [12] of electron emission from the Fermi level, while our quantum calculation includes emission from all occupied conduction-band levels. Our quantum-mechanical [Fig. 3(a)] and the classical calculations in [12] [Fig. 3(e)] also show a pronounced difference in the electron-spectral-yield distributions along the streaking traces, i.e., in the delay-dependent photoelectron dispersion. In addition to the neglect of photoemission from levels below the Fermi energy in Ref. [12], this difference is due the classical simulation modeling photoemission with equal probability from the entire surface of the nanosphere and over the entire XUV-pulse spectrum, while the quantum mechanical evaluation of the

transition amplitude for photoemission (4) weighs different emission locations, initial states, and final photoelectron states unequally. Qualitatively, this discrepancy can be accounted for by considering the energy dependence of the XUV photoemission cross section [33], shown in Fig. 3(f).

Figures 4(a) and 4(b) compare our simulated spectra for 720 and 530 nm streaking pulses for calculations that exclude the induced plasmonic field. All other parameters are the same as in Figs. 3(a) and 3(b). For a quantitative assessment of the induced-plasmonic-field effect on streaked photoemission spectra, we compare in Figs. 4(c) and 4(d) the CoE of the spectra in Figs. 3(a) and 3(b) with the spectra in Figs. 4(a) and Fig. 4(b), revealing a significant streaking-amplitude increase and streaking phase shift caused by the induced plasmonic field. The amplitude enhancement is consistent with the increase of the photoelectron's drift energy in the plasmonically enhanced streaking field.

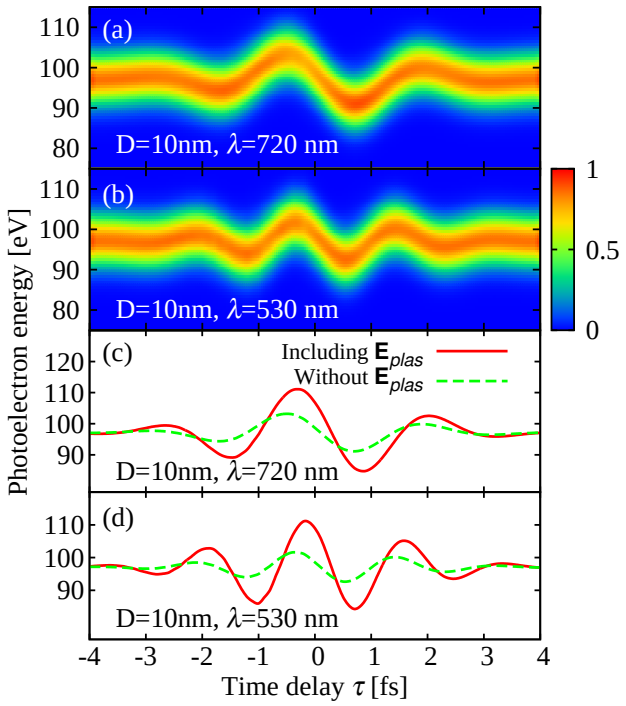

Figure 4. (Color online) Streaked XUV photoemission spectra for streaking-field wavelengths λ of (a) 720 nm and (b) 530 nm *without* inclusion of the induced plasmonic field for 10 nm diameter Au nanospheres. Streaking and XUV-pulse parameters are the same as in Fig. 3(a) and 3(b). Corresponding centers of energy for (c) $\lambda = 720$ nm and (d) $\lambda = 530$ nm with (solid red line) and without (dashed green line) inclusion of the induced plasmonic field. The linear color/gray scale is the same as in Fig. 3.

Figure 5(a) displays the plasmonic-field enhancement as a function of the streaking-pulse wavelength. The red solid line represents the electric field-strength enhancement $\eta(\mathbf{r}_p)$ at the poles as shown in Fig. 2(a). The

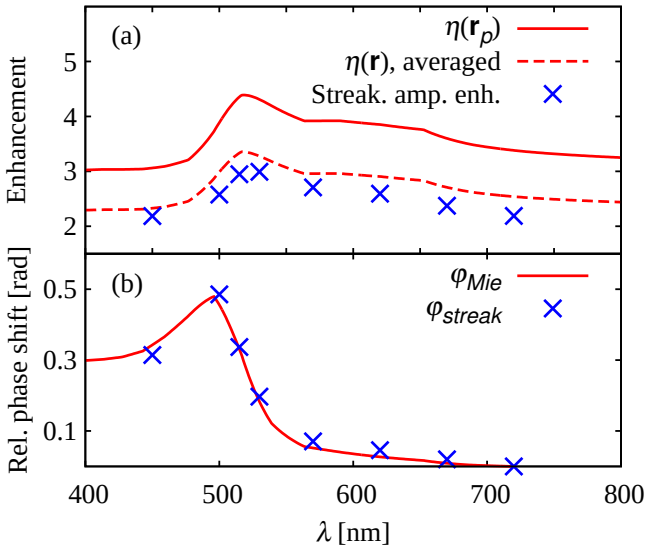

Figure 5. (Color online) Retrieval of the (a) plasmonic electric-field enhancement and (b) phase shift φ_{Mie} caused by the induced plasmonic field for 10 nm diameter Au nanospheres from streaked photoemission spectra as a function of the streaking-pulse wavelength. The red solid lines represent calculated electric-field enhancements and phase shifts at the electric poles of the nanosphere. The red dashed line shows a weighted average over the nanoparticle surface of the electric-field enhancement. Crosses indicate plasmonic streaking-amplitude enhancements and phase shifts obtained from streaked photoemission spectra.

dashed line represents the field enhancement at the surface averaged over the nanosphere surface with the weight factor $|\cos\theta|^2$, approximating the total electric-field distribution as dipolar. The crosses show the enhancement of streaking-oscillation amplitudes obtained as the ratio of photoemission yields calculated with and without including the plasmonic field. It resembles the shape of the averaged electric-field enhancement over one wavelength octave and maps the plasmonic resonance at 530 nm.

The solid red curve in Fig. 5(b) displays the plasmonic phase shift $\Delta\phi(\mathbf{r}_p)$ of Fig. 2(b) for 10 nm diameter Au nanospheres as a function of λ relative to the phase shift at $\lambda = 720$ nm,

$$\varphi_{Mie}(\lambda) = \Delta\phi(\mathbf{r}_p)\big|_{\lambda} - \Delta\phi(\mathbf{r}_p)\big|_{720\ \mathrm{nm}}. \qquad (8)$$

Averaging over all directions with weight $|\cos\theta|^2$ does not affect φ_{Mie} on the scale of Fig. 5(b). This angular independence of φ_{Mie} differs from the averaging-dependent amplitude enhancement in Fig. 5(a). This opposite averaging behavior is is due to the phase shift remaining approximately homogeneous near the surface, as long as the nanospheres is small compared to the wavelength of the streaking pulse, even though the plasmonic field enhancement is spatially inhomogeneous. The crosses indicate differences $\Delta\phi_{streak}$ of the phases between the CoEs of streaked photoemission spectra calculated with and

without the plasmonic field relative to their values at $\lambda = 720$ nm,

$$\varphi_{streak}(\lambda) = \Delta\phi_{streak}\big|_{\lambda} - \Delta\phi_{streak}\big|_{720\ \mathrm{nm}}. \quad (9)$$

The agreement between the retrieved phases $\varphi_{streak}(\lambda)$ and the Mie-theory-calculated phase shifts $\varphi_{Mie}(\lambda)$ indicates that phase information of the induced plasmonic field can be derived from streaked photoemission spectra. The successful reconstruction of the plasmonic phase also provides evidence for the accumulation of λ-independent contributions $\Delta\phi_{prop}$ during the propagation of photoelectrons. Writing the net accumulated plasmonic streaking phase difference as

$$\Delta\phi_{streak}\big|_{\lambda} = \Delta\phi(\mathbf{r}_p)\big|_{\lambda} + \Delta\phi_{prop}, \quad (10)$$

yields $\varphi_{streak}(\lambda) = \varphi_{Mie}(\lambda)$. The plasmonic streaking phase shift thus corresponds to the time delay of the collective electronic motion's response to the driving pulse. The maximum streaking phase shift at the plasmon resonance in Fig. 5(b) of about 0.5 rad corresponds to a delay of the collective electronic response to the driving streaking field $\mathbf{E}_{inc}$ of 130 as.

To conclude, we developed a quantum-mechanical model and numerically simulated streaked photoelectron emission from Au nanospheres. Our simulated spectra reveal a plasmonic streaking-amplitude enhancement and phase shift relative to calculations that exclude the induced plasmonic enhancement of the incident streaking-pulse electric field. For streaking-field wavelengths between 450 and 720 nm, our photoemission spectra retrace the enhancement and phase shift of the classically calculated plasmonic near-field. Our quantum-mechanical simulations thus substantiate previous suggestions based on classical simulations [6, 6, 12–14] to use streaked photoelectron spectroscopy for imaging the dielectric response and plasmonic fields near nanoparticle surfaces.

This work was supported in part by the NSF Experimental Program to Stimulate Competitive Research (EPSCoR), NSF Grant No. PHY 1464417, and the Chemical Sciences, Geosciences, and Biosciences Division, Office of Basic Energy Sciences, Office of Science, U.S. DOE.

[1] H. Hutter and J. H. Fendler, Adv. Mater. **16**, 1685 (2004).
[2] M. I. Stockman, Physics Today **64**, 29 (2011).
[3] M. I. Stockman, M. F. Kling, U. Kleineberg, and F. Krausz, Nat. Photonics **1**, 539 (2007).
[4] A. Kinkhabwala, Z. Yu, S. Fan, Y. Avlasevich, K. Müllen, and W. E. Moerner, Nat. Photonics **3**, 654 (2009).
[5] S. L. Stebbings, F. Süßmann, Y. Y. Yang, A. Scrinzi, M. Durach, M. I. Stockman, and M. F. Kling, New J. Phys. **13**, 073010 (2011).
[6] E. Skopalová, D. Y. Lei, T. Witting, C. Arrell, F. Frank, Y. Sonnefraud, S. A. Maier, J. W. G. Tisch, and J. P Marangos, New. J. Phys. **13**, 083003 (2011).
[7] M. Becker, W. Huang, H. Batelaan, E.J. Smythe, and F. Capasso, Ann. der Phys. (Berlin) **525**, L6 (2013).
[8] S. Kim, J. Jin, Y.-J. Kim, I.-Y. Park, Y. Kim, and S.-W. Kim, Nature **485**, E1(2012).
[9] P. Dombi, A. Hörl, P. Rácz, I. Márton, A. Trügler, J. R. Krenn, and U. Hohenester, Nano Lett. **13**, 2(2013).
[10] S. Zherebtsov, *et al.*, Nature Phys. **7**, 656 (2011).
[11] S. A. Maier and H. A. Atwater, J. Appl. Phys. **98**, 011101 (2005).
[12] F. Süßmann and M. F. Kling, Phys. Rev. B **84**, 121406 (2011).
[13] F. Kelkensberg, A. F. Koenderink, and M. J. J. Vrakking, New J. Phys. **14**, 093034 (2012).
[14] A. G. Borisov, P. M. Echenique, and A. K. Kazansky, New J. Phys. **14**, 023036 (2012).
[15] J. S. Prell, L. J. Borja, D. M. Neumark, and S. R. Leone, Ann. der Phys. (Berlin) **525**, 151 (2013).
[16] U. Thumm, Q. Liao, E. M. Bothschafter, F. Süßmann, M. F. Kling, and R. Kienberger, in: *Fundamentals of photonics and physics*, D. L. Andrew (ed.), (Wiley, New York 2015), Chapter 13.
[17] G. Mie, Ann. Phys. **25**, 377 (1908).
[18] E. C. Le Ru and P. G. Etchegoin, *Principles of surface-enhanced Raman spectroscopy and related plasmonic effects* (Elsevier, Oxford, 2009).
[19] X. Zhang, Y. L. Chen, R.-S. Liu, and D. P. Tsai, Rep. Prog. Phys. **76**, 046401 (2013).
[20] M. T. Sheldon, J. van de Groep, A. M. Brown, A. Polman, and H. A. Atwater, Science **346**, 828 (2014).
[21] F. Krausz and M. I. Stockman, Nat. Photonics **8**, 205 (2014).
[22] S. R. Leone, *et al.*, Nat. Photonics **8**, 162 (2014).
[23] C. Lemell, B. Solleder, K. Tőkési, and J. Burgdörfer, Phys. Rev. A **79**, 062901 (2009).
[24] Q. Liao and U. Thumm, Phys. Rev. Lett. **112**, 023602 (2014).
[25] C.-H. Zhang and U. Thumm, Phys. Rev. A **84**, 065403 (2011).
[26] Q. Liao and U. Thumm, Phys. Rev. A **89**, 033849 (2014).
[27] D. W. Lynch and D. R. Hunter in *Handbook of optical constants of solids*, E.D. Palik (ed.) (Academic Press, Orlando, FL, 1985), p. 275.
[28] J. A. Stratton, *Electromagnetic theory* (Wiley, Hoboken, NJ, 2007).
[29] S. Link and M. A. El-Sayed, J. Phys. Chem. B **103**, 4212 (1999).
[30] W. M. Haynes, *CRC handbook of chemistry and physics*, 96th ed. (CRC Press, Boca Raton, FL, 2015).
[31] A. Sekiyama, *et al.*, New J. Phys. **12**, 043045 (2010).
[32] S. Tanuma, C. J. Powell, and D. R. Penn, Surf. Interface Anal. **43**, 689 (2011).
[33] E. Merzbacher, *Quantum mechanics*, (Wiley, New York, 1998), p. 501.